Electronic Supplementary Material (ESI) for Organic Chemistry Frontiers.

Pillar[5]arene-based artificial light-harvesting system with red emission for high-resolution imaging of latent fingerprints

Tangxin Xiao[a,*], Liangliang Zhang[a], Dengli Chen[a], Qiaona Zhang[a], Qi Wang[b], Zheng-Yi Li[a] and Xiao-Qiang Sun[c]

[a]School of Petrochemical Engineering, Changzhou University, Changzhou 213164, China

E-mail: xiaotangxin@cczu.edu.cn

[b]State Key Laboratory for Organic Electronics and Information Displays & Institute of Advanced Materials (IAM), Nanjing University of Posts & Telecommunications, Nanjing 210023, China

[c]Institute of Urban & Rural Mining, Changzhou University, Changzhou 213164, China

Table of contents

1. Materials, methods, and abbreviations

General

All chemicals, reagents and solvents were purchased from commercial suppliers and used, unless otherwise stated, without further purification. If needed, solvents were dried by literature known procedures. All yields were given as isolated yields. The synthesis of **WP5** was according to the literature procedures.[S1]

NMR spectroscopy

The ^{1}H NMR spectra were recorded in a Bruker AVANCE III (300 MHz) spectrometer and calibrated against the residual proton signal or natural abundance carbon resonance of the used deuterated solvent from tetramethylsilane (TMS) as the internal standard. The chemical shifts δ are indicated in ppm and the coupling constants *J* in Hz. The multiplicities are given as s (singlet), d (doublet), t (triplet), m (multiplet), and br (broad).

Mass spectrometry

High-resolution electrospray ionization mass spectra (HR-ESI-MS) were recorded on an Agilent Technologies 6540 UHD Accurate-Mass. Matrix-assisted laser desorption/ionization time-of-flight (MALDI-TOF) mass spectra were recorded in positive-ion mode using an Autoflex III (Bruker Daltonics, Germany) time-of-flight mass spectrometer.

Melting point determination

Melting points were determined on a SGW X-4B melting point apparatus.

Transmission electron microscope (TEM)

TEM investigations were carried out on a JEM-2100 instrument.

Dynamic light scattering (DLS)

DLS were measured on a Zetasizer Nano ZS ZEN3600.

UV-vis spectroscopy

The UV-vis absorption spectra were measured on a Perkin Elmer Lambda 35 UV-vis Spectrometer.

Fluorescence spectroscopy

Fluorescence measurements were performed on an Agilent Cary Eclipse spectrofluorometer.

Fluorescence lifetimes

The fluorescence lifetimes were measured employing time correlated single photon counting on a FLS980 instrument with a pulsed xenon lamp. Analysis of fluorescence decay curves were subjected to fit a bi-exponential decay. The instrument response function (IRF) measures the scattering of laser excitation from non-fluorescent control samples to determine the fastest possible response of the detectors.

Fluorescent quantum yields

The quantum yields were carried out on a FLS980 instrument with the integrating sphere.

CIE coordinates

The CIE (Commission Internationale de l'Eclairage) 1931 coordinates were calculated with the method of color matching functions.

Fingerprints collection and analysis

20 mL solution of **WP5⊃G**@NiR ([**G**] = 5×10^{-5} M, [**G**]/[**WP5**] = 1/0.3, [**G**]/[NiR] = 100/1) was concentrated to 5 mL, and then 1 g MMT powder was added. After ultrasonication for 10 minutes, the solvent was evaporated using a rotary evaporator. The fingerprint powder was then dried overnight in a vacuum oven and stored in a dry container. Volunteers were asked to rub their fingers on their foreheads and press their fingers against a selected substrate surface. These substrates (except petal) were thoroughly cleaned and dried in a vacuum dryer for 48 hours before being stored in a dryer. First, applying fluorescent fingerprint powder directly and evenly to the surface of the substrate, gently apply it with a feather brush, and then blow off excess powder with a washing ear ball. The images of fingerprints were recorded with Mi 11 smartphone under the irradiation of UV-lamp (365 nm). The fingerprint gray scale was analyzed by Image J 7.0.

Abbreviations

N_2 = nitrogen; CAC = critical aggregation concentration; NPs = nanoparticles; M = mol/L; LHS = light-harvesting system; DLS = dynamic light scattering; MMT = montmorillonite.

2. Synthesis of G

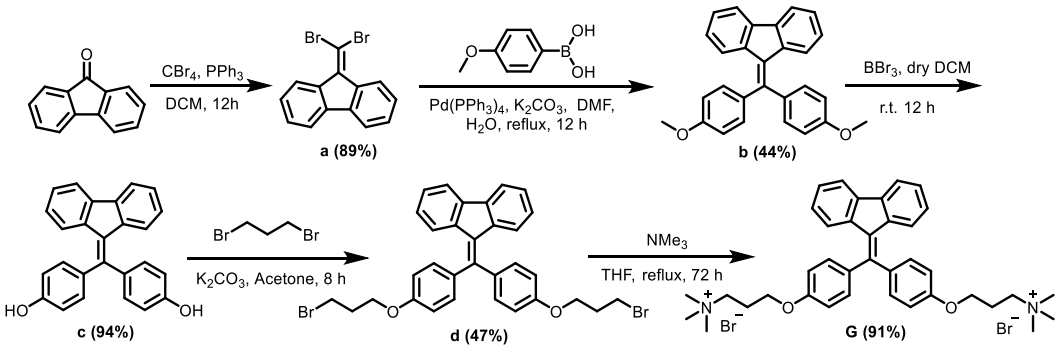

Scheme S1. Synthesis of **G**.

Compound **a**, **b** and **c** were prepared according to literature procedure.[S2]

Synthesis of compound d. Compound **c** (0.50 g, 1.4 mmol), 1,3-dibromopropane (0.85 g, 4.2 mmol), K_2CO_3 (0.60 g, 4.2 mmol) and acetone (20 mL) were combined in a 100 mL flask under an argon atmosphere. The reaction mixture was refluxed for 8 hours, then the reaction mixture was cooled to room temperature and partitioned between CH_2Cl_2 (50 mL) and H_2O (40 mL). The resulting mixture was separated, and the aqueous layer was extracted twice with CH_2Cl_2 (20 mL). The combined organic phase was dried over anhydrous Na_2SO_4, filtered, and concentrated in vacuo. The residue was purified by column chromatography (PE/DCM, 5/1) to afford compound **d** as a yellow solid (0.40 g, 47%). m. p.: 135-137 °C. ^{1}H NMR (300 MHz, $CDCl_3$, 298 K): δ (ppm) = 7.72 (d, *J* = 7.5Hz, 2H, Ar-*H*), 7.29-7.28 (m, 2H, Ar-*H*), 7.24-7.21 (m, 4H, Ar-*H*), 6.99-6.91 (m, 6H, Ar-*H*), 6.81 (d, *J* = 7.8 Hz, 2H, Ar-*H*), 4.17 (t, *J* = 5.7 Hz, 4H, -OC*H*$_2$-), 3.65 (t, *J* = 6.3 Hz, 4H, -C*H*$_2$Br), 2.41-2.33 (m, 4H, -C*H*$_2$-). ^{13}C NMR (75 MHz, $CDCl_3$, 298 K): δ (ppm) = 159.0, 145.4, 140.2, 139.1, 135.8, 133.3, 132.0, 127.2, 126.3, 124.6, 119.2. 114.6, 65.3, 32.4, 30.0. MALDI-TOF MS: *m/z* [M - e]$^+$ calcd for $[C_{32}H_{28}Br_2O_2]^+$ = 604.044 (^{79}Br^{81}Br), 602.046 (^{79}Br^{79}Br) and 606.041 (^{81}Br^{81}Br), found 604.298 (100%), 602.285 (50%) and 606.303 (55%); HR-ESI-MS: *m/z* [M + H]$^+$ calcd for $[C_{32}H_{29}Br_2O_2]^+$ = 605.0508, found 605.0487.

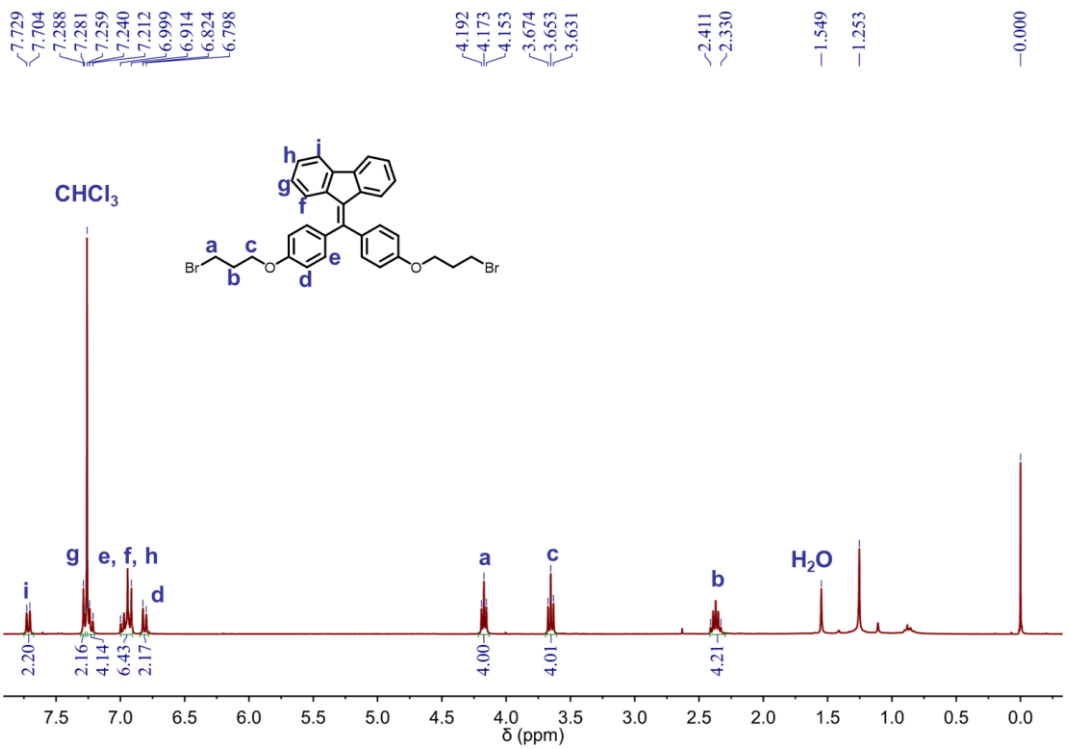

Fig. S1. ^{1}H NMR spectrum (300 MHz, $CDCl_3$, 298 K) of compound **d**.

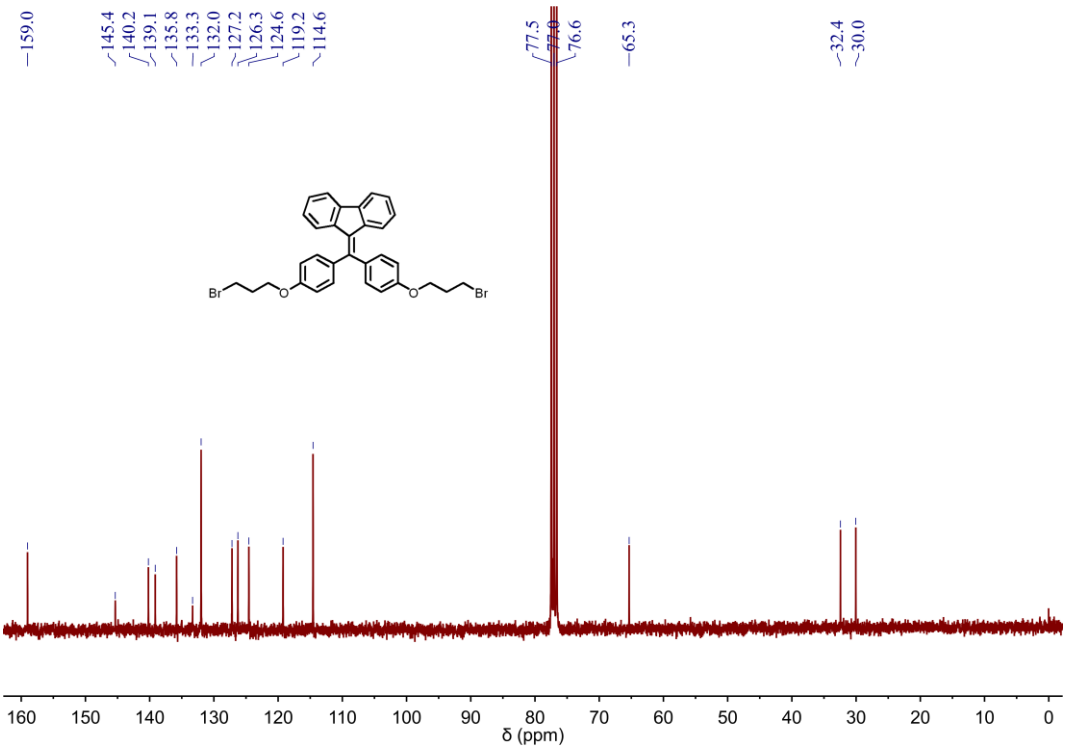

Fig. S2. ^{13}C NMR spectrum (75 MHz, $CDCl_3$, 298 K) of compound **d**.

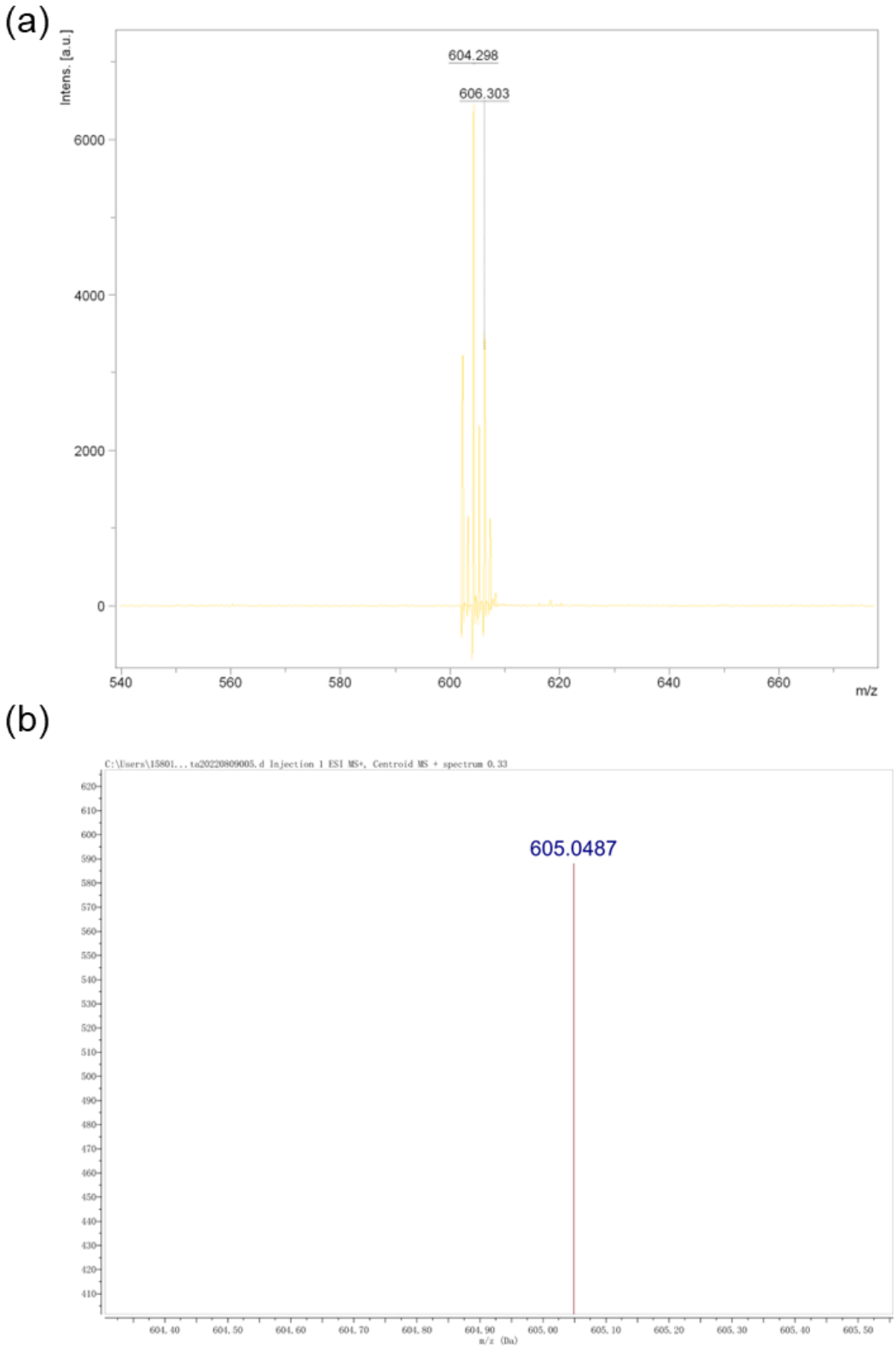

Fig. S3. (a) MOLDI-TOF-MS and (b) HR-MS (ESI, positive mode, MeOH) spectra of compound **d**.

Synthesis of G. A mixture of compound **d** (0.40 g, 0.67 mmol) and trimethylamine (1.6 mL, 6.7 mmol) was dissolved in 40 mL anhydrous THF in a 100 mL flask. The mixture was heated to reflux and stirred for 3 days. During this period, 1.6 mL of trimethylamine was added every day. After that, THF and extra triethylamine were evaporated. The residue was washed with petroleum ether, ethyl acetate and acetone to obtain a yellow solid (0.44 g, 91%). m. p.: 264-267 °C. ^{1}H NMR (300 MHz, DMSO-d_6, 298 K): δ (ppm) = 7.86 (d, J = 7.5 Hz, 2H, Ar-*H*), 7.30-7.24 (m, 6H, Ar-*H*), 7.07-6.95 (m, 6H, Ar-*H*), 6.63 (d, J = 8.1 Hz, 2H, Ar-*H*), 4.14 (t, J = 5.7 Hz, 4H, NCH_2-), 3.54 (t, J = 8.1 Hz, 4H, -OCH_2-), 3.31 (s, 18H, -N(CH_3)$_3$), 2.23 (m, 4H, -CH_2-). ^{13}C NMR (75 MHz, DMSO-d_6, 298 K): δ (ppm) = 159.0, 146.0, 140.1, 138.7, 135.6, 132.9, 131.6, 128.0, 126.9, 124.4, 120.2. 115.3, 65.3, 63.4, 52.8, 23.1. HR-ESI-MS: *m/z* [M – 2Br]$^{2+}$ calcd for [$C_{38}H_{46}N_2O_2$]$^{2+}$ = 281.1774, found 281.1773.

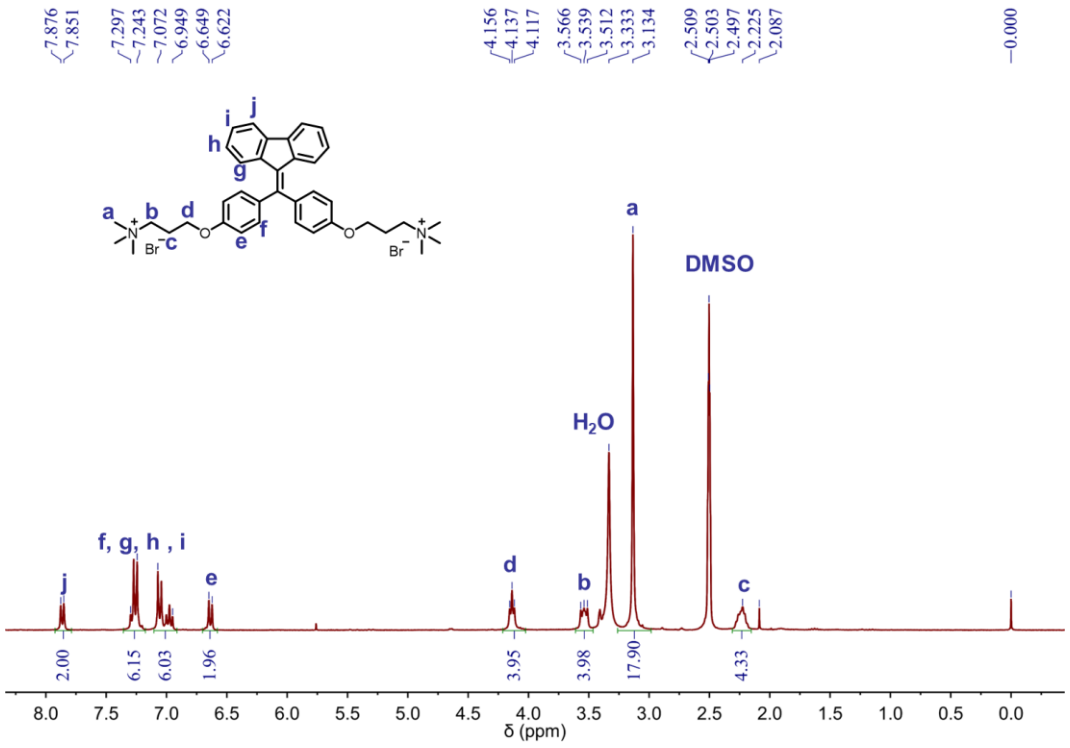

Fig. S4. ^{1}H NMR spectrum (300 MHz, DMSO-d_6, 298 K) of **G**.

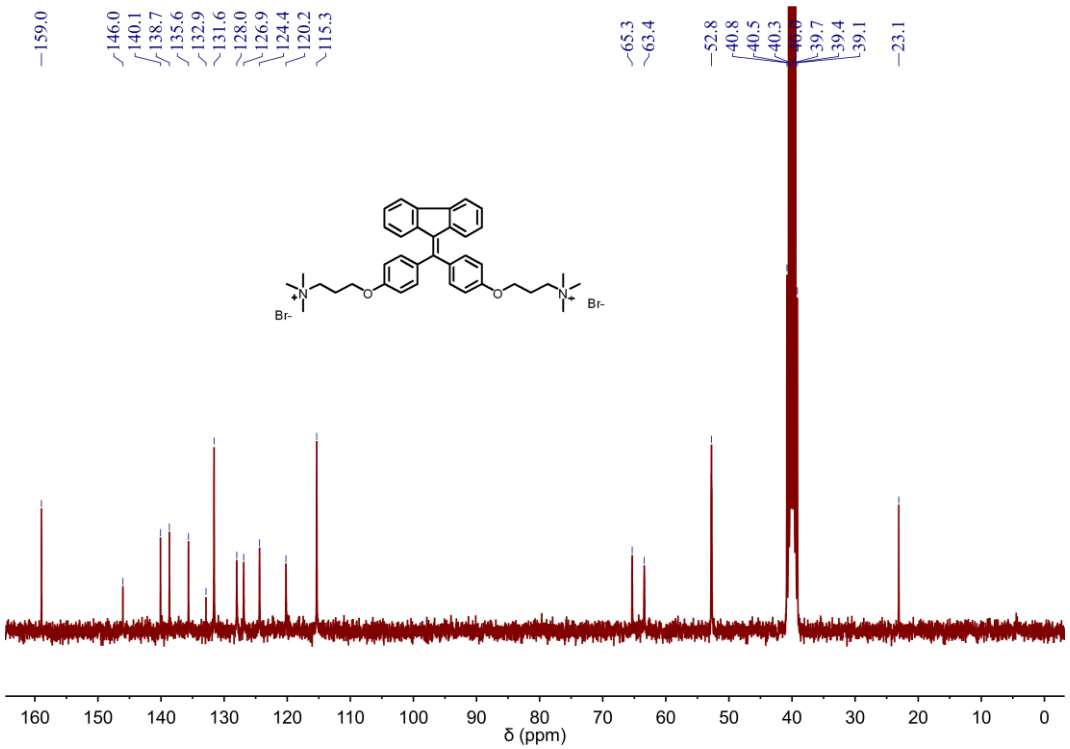

Fig. S5. ^{13}C NMR spectrum (75 MHz, DMSO-d_6, 298 K) of **G**.

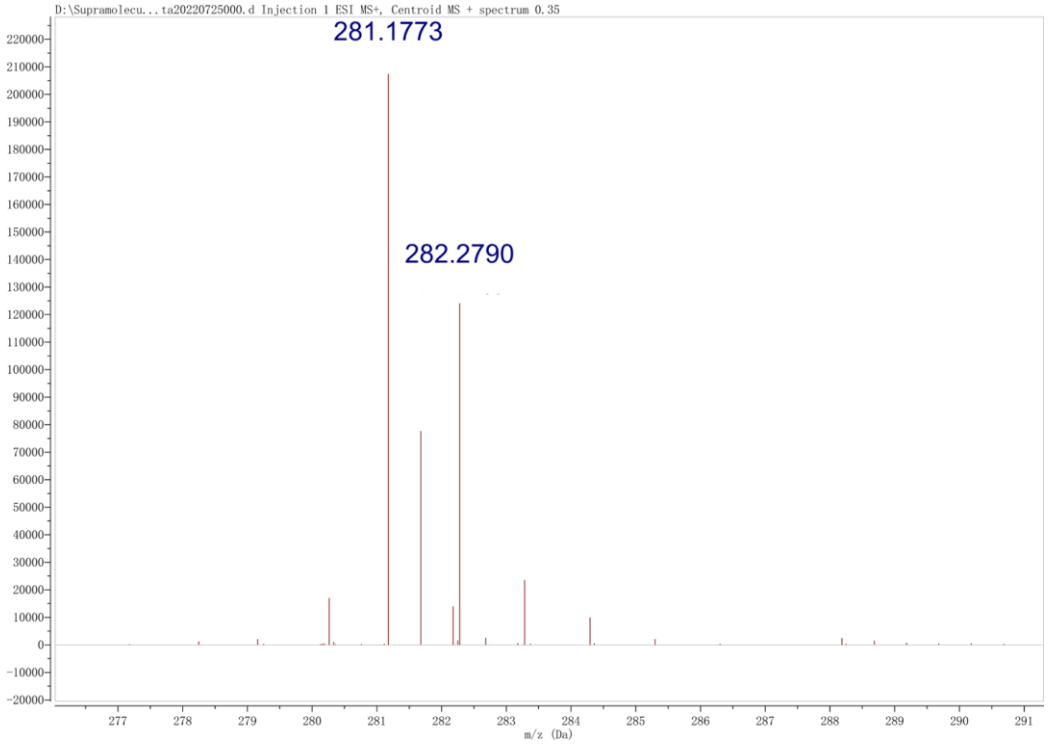

Fig. S6. HR-MS (ESI, positive mode, MeOH) spectrum of **G**.

3. AIE behavior of G

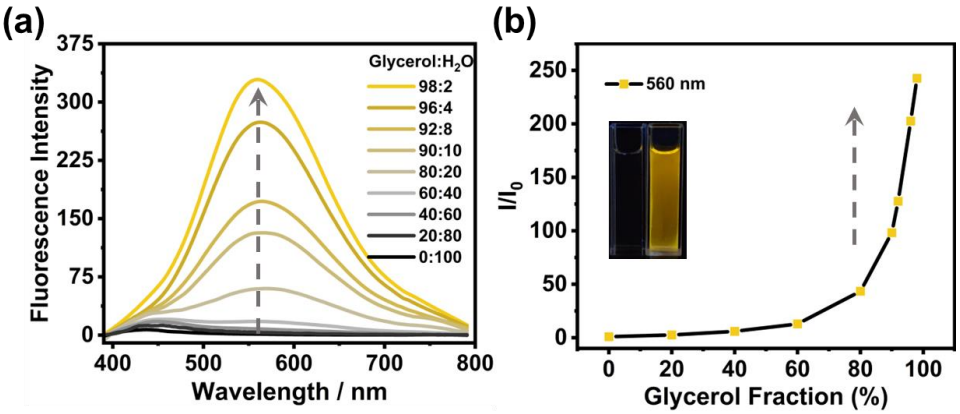

Fig. S7. (a) Fluorescence spectra of **G** in mixed glycerol/H_2O solvents at different vol% upon excitation at 370 nm. (b) Fluorescence intensity of **G** at 560 nm in the presence of different factions of glycerol, inset: fluorescence images of **G** in pure H_2O (left) and glycerol (right). [**G**] = 1×10^{-4} M.

4. Quantum yields of G in the presence of different macrocycles

Table S1. Fluorescence quantum yields ($\mathbf{\Phi}_{f(abs)}$) of **G**, α-CD/**G**, β-CD/**G**, γ-CD/**G**, CB[6]/**G**, CB[7]/**G**, CB[8]/**G** and **WP5⊃G** in water. λ_{ex} = 370 nm, [**G**] = 2×10^{-5} M. Molar ratio of [host]/[guest] in all samples is 1 : 1.

Sample	Fluorescence quantum yields ($\Phi_{f(abs)}$)
G	0.39%
α-CD/**G**	0.21%
β-CD/**G**	0.74%
γ-CD/**G**	0.55%
CB[6]/**G**	0.66%
CB[7]/**G**	0.90%
CB[8]/**G**	0.57%
WP5⊃G	7.00%

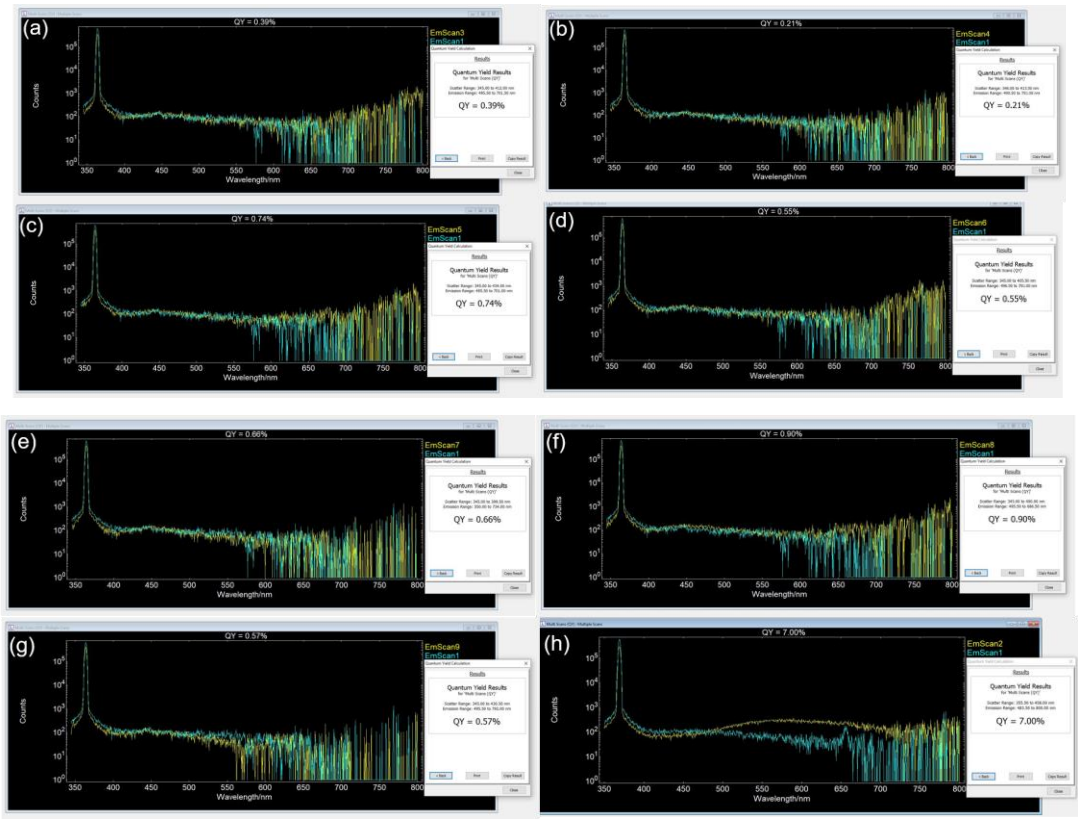

Fig. S8. Absolute fluorescence quantum yields of (a) **G** (2×10^{-5} M) and in the presence of (b) α-CD, (c) β-CD, (d) γ-CD, (e) CB[6], (f) CB[7], (g) CB[8], and (h) **WP5** in water at 25 °C, λ_{ex} = 370 nm.

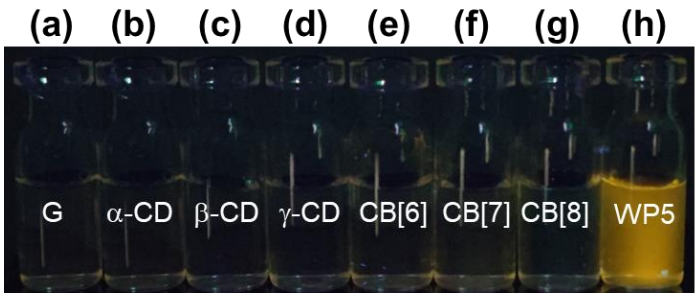

Fig. S9. Photographs of (a) **G** (2×10^{-5} M) and in the presence of (b) α-CD, (c) β-CD, (d) γ-CD, (e) CB[6], (f) CB[7], (g) CB[8], and (h) **WP5** in water at 25 °C under UV lamp irradiation at 365 nm.

5. Host-guest complexation of WP5 and G_M

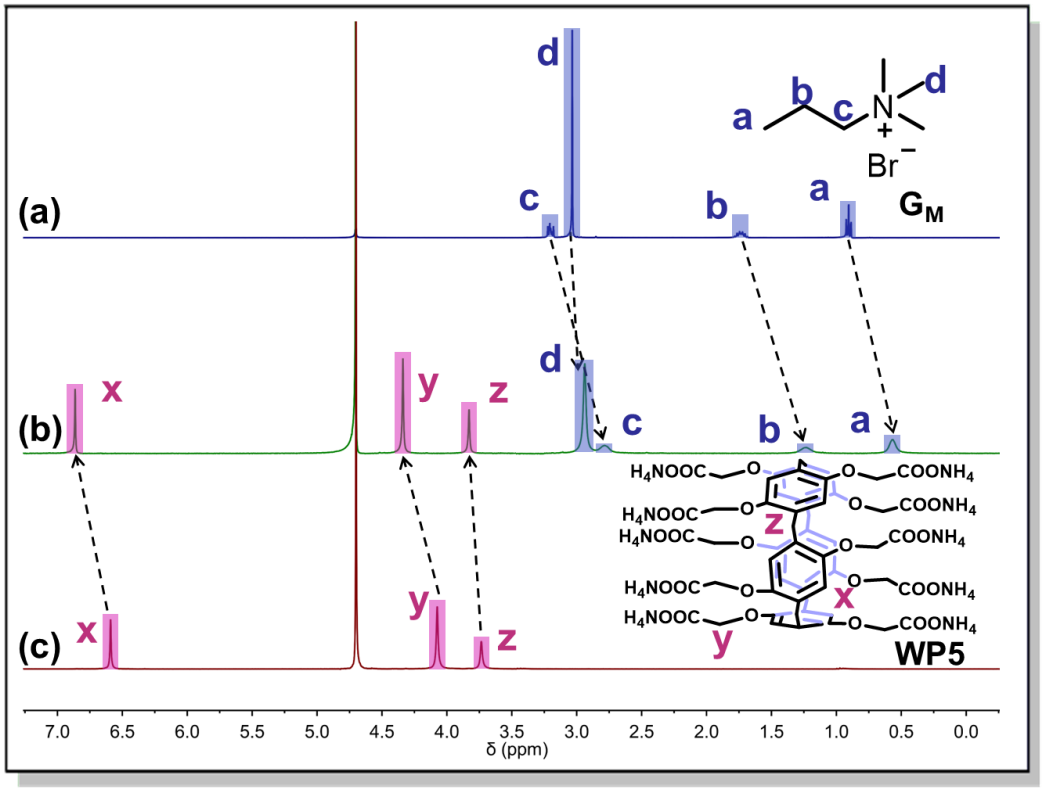

Fig. S10. ^{1}H NMR (400 MHz, D_2O, 298 K) spectra: (a) $\mathbf{G_M}$ (4.0 mM), (b) **WP5** (4.0 mM) and $\mathbf{G_M}$ (4.0 mM), and (c) **WP5** (4.0 mM).

6. Self-assembly of WP5 and G

(1) Determination of the CAC of **G**

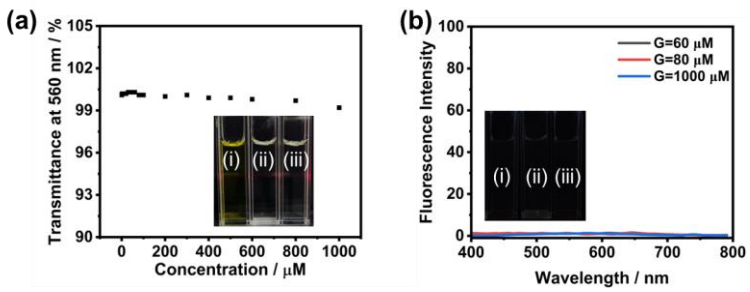

Fig. S11. (a) Optical transmittance of **G** at 560 nm in different concentrations (0.001-1.0 mM) in water. Inset: laser irradiation showed no Tyndall effects of (i) **G** = 1.0 mM, (ii) **G** = 0.08 mM and (iii) **G** = 0.06 mM. (b) Fluorescence spectra of **G** in pure water. Inset: fluorescence photographs of (i) **G** = 1.0 mM, (ii) **G** = 0.08 mM and (iii) **G** = 0.06 mM, which showed no fluorescence emission.

(2) Determination of the best molar ratio of **WP5⊃G** by transmittance

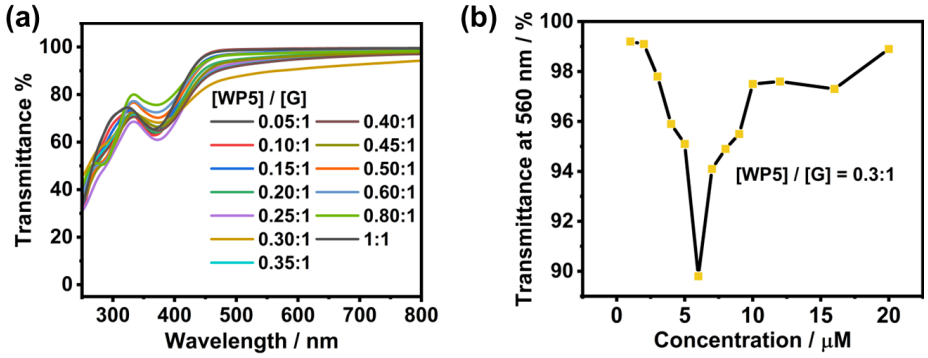

Fig. S12. (a) Optical transmittance of **G** (20 μM) upon the titration of **WP5** (1-20 μM) at 25 °C in water. (b) Optical transmittance of **G** (20 μM) at 560 nm upon increasing the concentration of **WP5** (1-20 μM) at 25 °C in water.

(3) Fluorescence titration spectra of the **WP5⊃G**

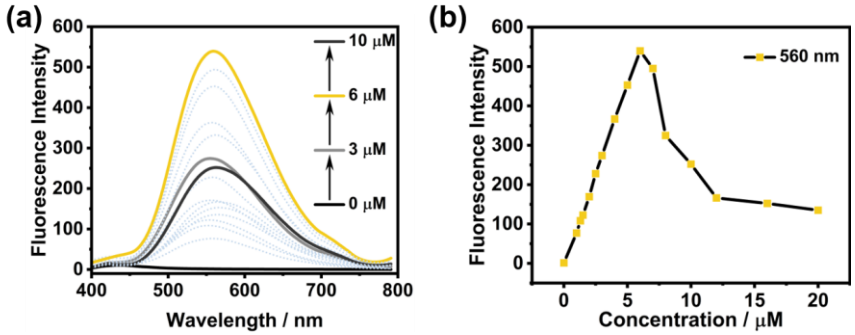

Fig. S13. (a) Fluorescence spectra of **G** (2×10^{-5} M) upon the titration of **WP5**. (b) Fluorescence intensity of **G** (2×10^{-5} M) at 560 nm upon the addition of **WP5**, λ_{ex} = 370 nm.

(4) Determination of the CAC of **WP5⊃G**

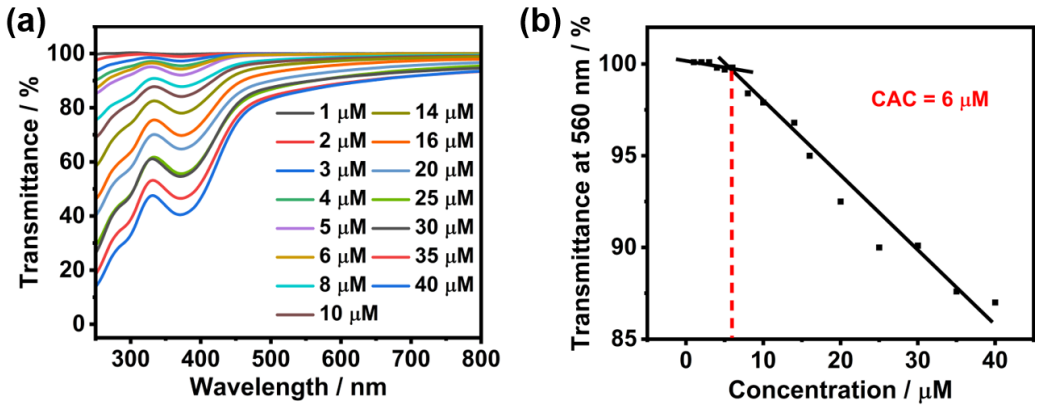

Fig. S14. (a) Optical transmittance of the **WP5⊃G** assembly with a fixed molar ratio of [**WP5**] : [**G**] = 0.3 : 1 at different concentrations of **G** from 1 to 40 μM. (b) Concentration-dependent optical transmittance of the **WP5⊃G** aggregates at 560 nm with a fixed molar ratio of [**WP5**] : [**G**] = 0.3 : 1.

7. Fluorescence lifetimes and quantum yields of LHS

Table S2. Fluorescence lifetimes of **WP5⊃G** and **WP5⊃G**@NiR monitored at 560 nm upon excitation at 370 nm in aqueous solution. [**WP5**] = 6×10^{-6} M, [**G**] = 2×10^{-5} M, and [NiR] = 4×10^{-7} M, respectively.

Sample	τ_1	RW1%	τ_2	RW2%	τ	χ^2
WP5⊃G	0.93	61.71%	2.29	38.29%	1.62	1.112
WP5⊃G@NiR	0.82	32.04%	2.00	67.96%	1.45	1.130

Table S3. Fluorescence quantum yields ($\Phi_{f(abs)}$) of (a) **WP5⊃G**, (b) **WP5⊃G**@NiR. [**WP5**] = 6×10^{-6} M, [**G**] = 2×10^{-5} M, and [NiR] = 4×10^{-7} M, respectively.

Sample	Fluorescence quantum yields ($\Phi_{f(abs)}$)
WP5⊃G	10.72%
WP5⊃G@NiR (**WP5⊃G** : NiR = 50: 1)	14.69%

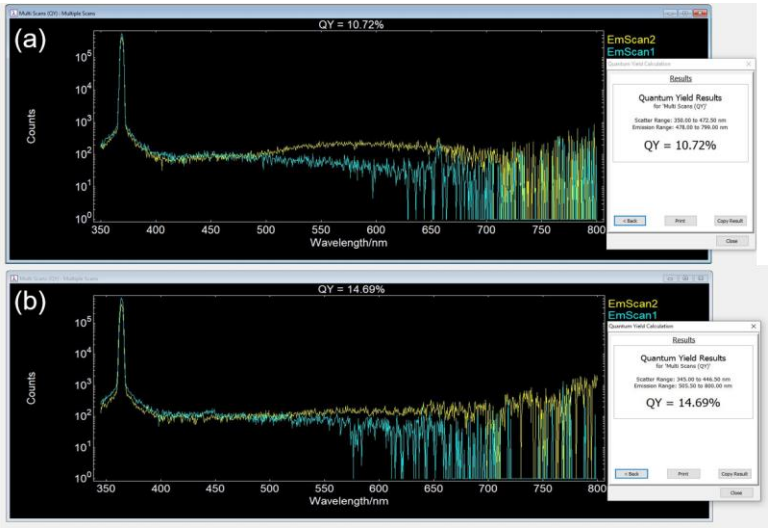

Fig. S15. Absolute fluorescence quantum yields ($\Phi_{f(abs)}$) of (a) **WP5⊃G**, (b) **WP5⊃G**@NiR upon excitation at 370 nm. [**WP5**] = 6×10^{-6} M, [**G**] = 2×10^{-5} M, and [NiR] = 4×10^{-7} M, respectively.

8. Energy-transfer efficiency calculation

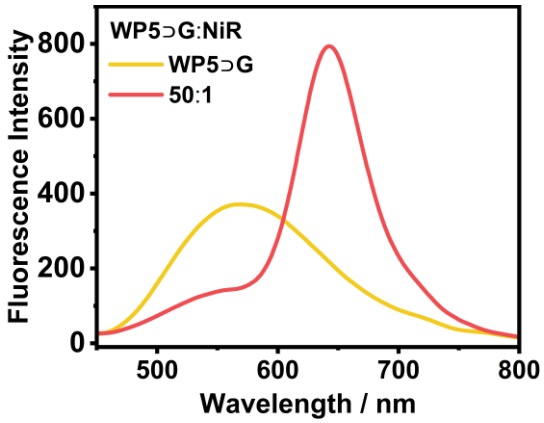

Fig. S16. Fluorescence spectra of **WP5⊃G** and **WP5⊃G**@NiR assembly upon excitation at 370 nm. **WP5⊃G** (yellow line), **WP5⊃G**@NiR (red line), respectively. [**WP5**] = 6×10^{-6} M, [**G**] = 2×10^{-5} M, and [NiR] = 4×10^{-7} M, respectively.

Energy-transfer efficiency (Φ_{ET}) was calculated from fluorescence spectra through the equation S1[S3]:

$$\Phi_{ET} = 1 - I_{DA}/I_D \text{ (eq. S1)}$$

Where I_{DA} and I_D are the fluorescence intensities of **WP5⊃G**@NiR (donor and acceptor) and **WP5⊃G** (donor) at 560 nm when excited at 370 nm, respectively.

The energy-transfer efficiency (Φ_{ET}) was calculated to be 60.9% in water, measured under the condition of [**WP5**] = 6×10^{-6} M, [**G**] = 2×10^{-5} M, [NiR] = 4×10^{-7} M (λ_{ex} = 370 nm and λ_{em} = 560 nm).

Similarly, the Φ_{ET} of other **WP5⊃G**@NiR ratios can also be calculated according to this equation.

Table S4. Energy-transfer efficiency with different **WP5⊃G**/NiR ratio.

Sample	**Concentration, respectively**	**Energy-transfer efficiency (Φ_{ET})**
WP5⊃G@NiR (**WP5⊃G**: NiR = 50: 1)	**[WP5] =** 6×10^{-6} M **[G]** = 2×10^{-5} M [NiR] = 4×10^{-7} M	60.9%
WP5⊃G@NiR (**WP5⊃G**: NiR = 75: 1)	**[WP5]** =6×10^{-6} M **[G]** = 2×10^{-5} M [NiR] = 2.6×10^{-7} M	52.7%
WP5⊃G@NiR (**WP5⊃G**: NiR = 100: 1)	**[WP5]** = 6×10^{-6} M **[G]** = 2×10^{-5} M [NiR] = 2×10^{-7} M	38.5%
WP5⊃G@NiR (**WP5⊃G**: **ESY** = 200: 1)	**[WP5]** = 6×10^{-6} M **[G]** = 2×10^{-5} M [NiR] =1×10^{-7} M	30.1%
WP5⊃G@NiR (**WP5⊃G**: NiR = 300: 1)	**[WP5]** = 6×10^{-6} M **[G]** = 2×10^{-5} M [NiR] = 6.7×10^{-8} M	23.7%
WP5⊃G@NiR (**WP5⊃G**: NiR = 400: 1)	**[WP5]** = 6×10^{-6} M **[G]** = 2×10^{-5} M [NiR] = 5×10^{-8} M	19.39%
WP5⊃G@NiR (**WP5⊃G**: NiR = 600: 1)	**[WP5]** = 6×10^{-6} M **[G]** = 2×10^{-5} M [NiR] = 3.33×10^{-8} M	16.18%
WP5⊃G@NiR (**WP5⊃G**: NiR = 1000: 1)	**[WP5]** = 6×10^{-6} M **[G]** = 2×10^{-5} M [NiR] = 2×10^{-8} M	10.7%

9. Antenna effect (AE) calculation

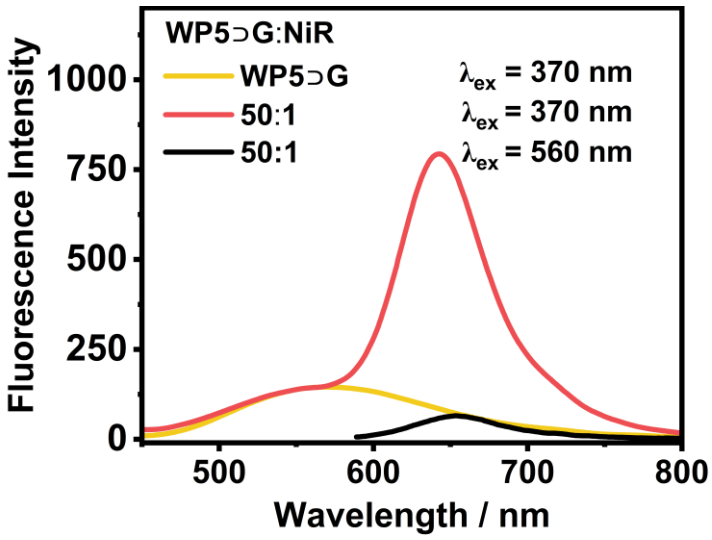

Fig. S17. Fluorescence spectra of **WP5⊃G** (yellow line) and **WP5⊃G**@NiR (red line) normalized at 560 nm, respectively, λ_{ex} = 370 nm. The black line represents the fluorescence spectrum of **WP5⊃G**@NiR, λ_{ex} = 560 nm. [**WP5**] = 6 × 10^{-6} M, [**G**] = 2 × 10^{-5} M, and [NiR] = 4 × 10^{-7} M, respectively.

The antenna effect (AE) was calculated based on the emission spectra using equation S2[S3]:

$$AE = I'_{DA,370}/I_{DA,560} = (I_{DA,370} - I_{D,370})/I_{DA,560} \text{ (eq. S2)}$$

Where $I_{DA,370}$ and $I_{DA,560}$ are the fluorescence intensities at 640 nm with the excitation of **WP5⊃G**@NiR at 370 nm and at 560 nm, respectively. $I_{D,370}$ refers to the fluorescence intensity of **WP5⊃G** NPs at 640 nm under excitation at 370 nm after its emission spectrum was normalized at 560 nm.

The antenna effect value was calculated as 21.79 in water, measured under the condition of [**WP5**] = 6 × 10^{-6} M, [**G**] = 2 × 10^{-5} M, and [NiR] = 1 × 10^{-7} M, respectively.

Similarly, the antenna effect of other **WP5⊃G**@NiR ratios was also calculated according to this equation.

Table S5. Antenna effect with different **WP5⊃G**@NiR ratios.

Sample	Concentration, respectively	Antenna Effect (AE)
WP5⊃G@NiR (**WP5⊃G**: NiR = 50: 1)	**[WP5] =** 5×10^{-6} M **[G]** = 2×10^{-5} M [NiR] = 4×10^{-7} M	12.35
WP5⊃G@NiR (**WP5⊃G**: NiR = 75: 1)	**[WP5]** = 5×10^{-6} M **[G]** = 2×10^{-5} M **[**NiR**]** = 2.6×10^{-7} M	13.74
WP5⊃G@NiR (**WP5⊃G**: NiR = 100: 1)	**[WP5]** = 5×10^{-6} M **[G]** = 2×10^{-5} M **[**NiR**]** = 2×10^{-7} M	17.66
WP5⊃G@NiR (**WP5⊃G**: NiR = 200: 1)	**[WP5]** = 5×10^{-6} M **[G]** = 2×10^{-5} M **[**NiR**]** = 1×10^{-7} M	21.79
WP5⊃G@NiR (**WP5⊃G**: NiR = 300: 1)	**[WP5]** = 5×10^{-6} M **[G]** = 2×10^{-5} M **[**NiR**]** = 5×10^{-8} M	19.51
WP5⊃G@NiR (**WP5⊃G**: NiR = 400: 1)	**[WP5]** = 6.7×10^{-6} M **[G]** = 2×10^{-5} M **[**NiR**]** = 5×10^{-8} M	20.98
WP5⊃G@NiR (**WP5⊃G**: NiR = 600: 1)	**[WP5]** = 5×10^{-6} M **[G]** = 2×10^{-5} M **[**NiR**]** = 3.3×10^{-8} M	20.29
WP5⊃G@NiR (**WP5⊃G**: NiR = 1000: 1)	**[WP5]** = 5×10^{-6} M **[G]** = 2×10^{-5} M **[**NiR**]** = 2×10^{-8} M	18.74

10. Stern−Volmer equation and CIE chromaticity diagram

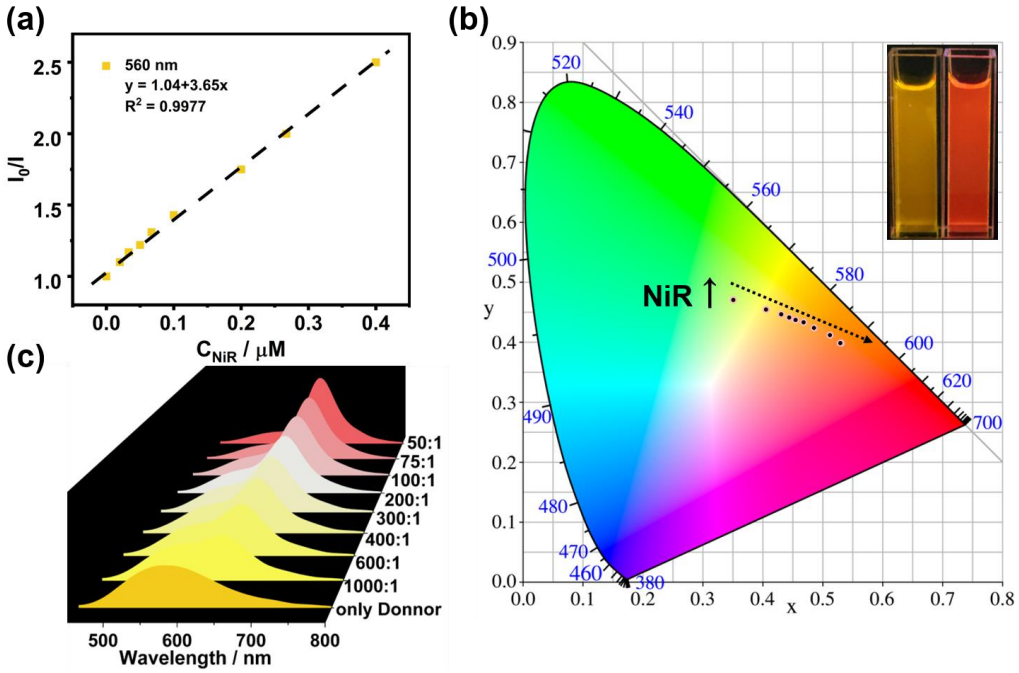

Figure S18. (a) Stern–Volmer plot of the **WP5⊃G**@NiR system. (b) The CIE chromaticity diagram of photoluminescence color changes by varying the ratios of the chromophores. (c)The fluorescence spectra of **WP5⊃G** in water with different concentrations of NiR.

11. Latent fingerprints imaging

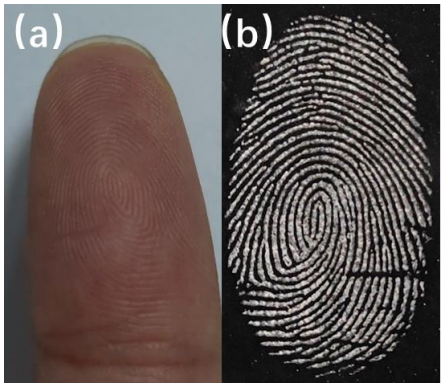

Fig. S19. (a) Fingerprint picture of an adult male volunteer. (b) Day light LFP images using **WP5⊃G**@NiR-MMT powder.

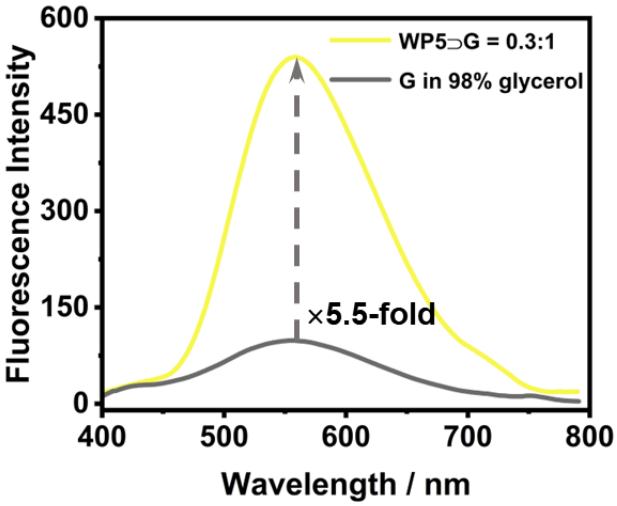

Fig. S20. Fluorescence spectra of **WP5⊃G** in water and **G** in mixed glycerol/H_2O solvents. λ_{ex} = 370 nm, [**WP5**] = 6 × 10^{-6} M, [**G**] = 2 × 10^{-5} M.

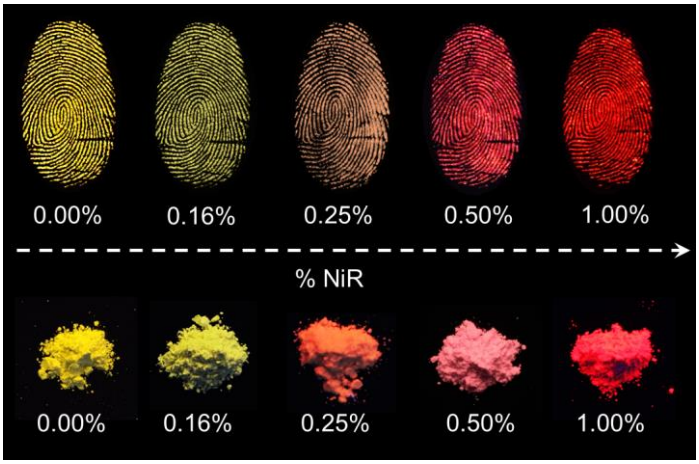

Fig. S21. Fluorescent fingerprint images developed by the LHS with different NiR contents.

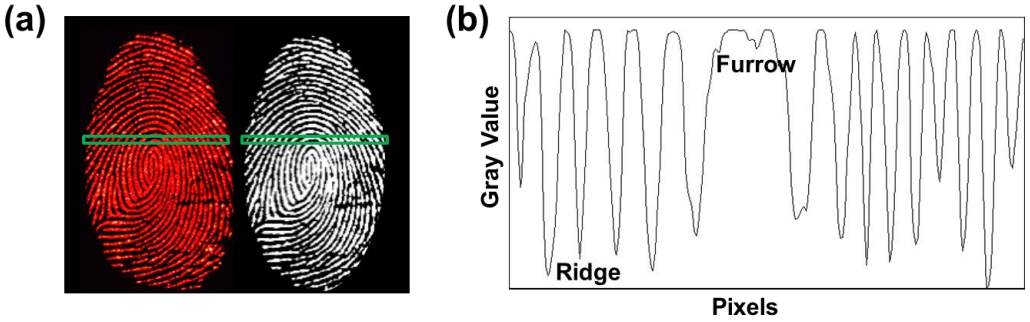

Fig. S22. (a) Fluorescence (left) and grayscale (right) images, and (b) resolution analysis of latent fingerprints stained by **WP5⊃G**@NiR-MTT powder on glass plate.

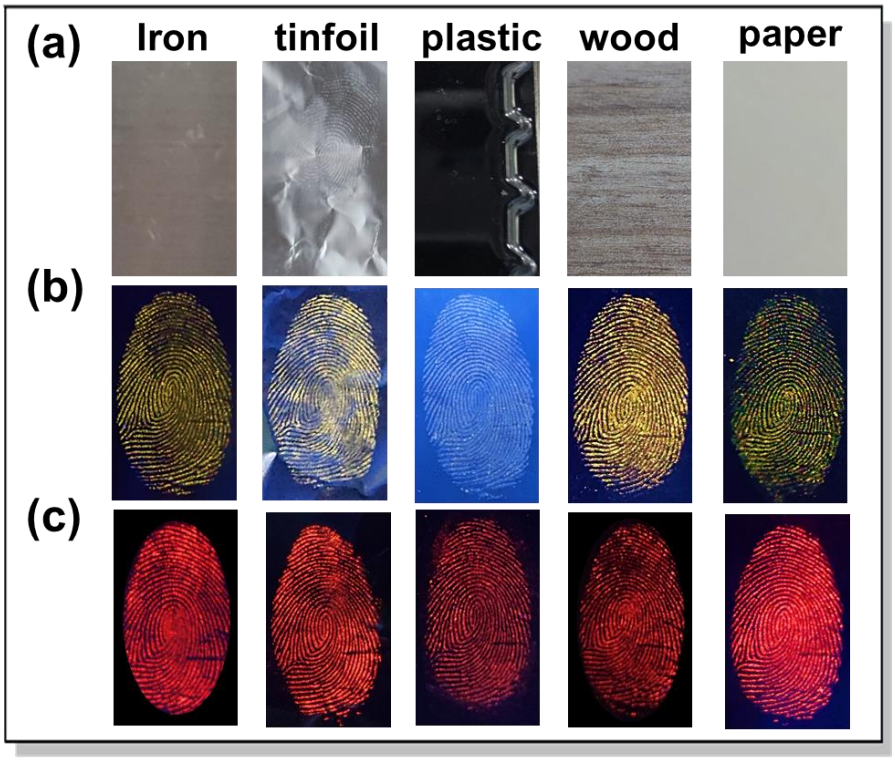

Fig. S23. Images of developed LFPs on the surface of different substrates. (a) Photographs of different raw substrates; Fluorescent LFPs images stained with (b) **WP5⊃G**-MMT and (c) **WP5⊃G**@NiR-MTT under UV light (365 nm).

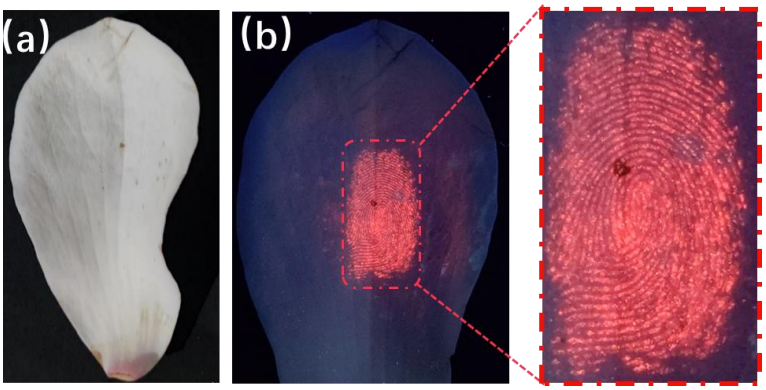

Fig. S24. LFP images of a magnolia flower petal developed by **WP5⊃G**@NiR-MMT powder under (a) daylight and (b) 365 nm UV light.

12. References

[S1] C. Ding, Y. Liu, T. Wang and J. Fu, Triple-stimuli-responsive nanocontainers assembled by water-soluble pillar[5]arene-based pseudorotaxanes for controlled release, *J. Mater. Chem. B*, **2016**, *4*, 2819-2827.

[S2] T. Xiao, J. Wang, Y. Shen, C. Bao, Z.-Y. Li, X.-Q. Sun and L. Wang, Preparation of a fixed-tetraphenylethylene motif bridged ditopic benzo-21-crown-7 and its application for constructing AIE supramolecular polymers, *Chin. Chem. Lett.* **2021**, *32*, 1377-1380.

[S3] M. Hao, G. Sun, M. Zuo, Z. Xu, Y. Chen, X. Y. Hu and L. Wang, A supramolecular artificial light-harvesting system with two-step sequential energy transfer for photochemical catalysis, *Angew. Chem. Int. Ed.* **2020**, *59*, 10095-10100.